FLOW FEATURES OF HIGHLY-SWEPT WINGS AT SUBSONIC AND SUPERSONIC SPEEDS

P. R. Ashill, J. L. Fulker, M. J. Simmons, C. J. Betts
Royal Aerospace Establishment,
Bedford, England

Abstract

A combined, experimental-theoretical investigation of flows over highly-swept, delta wings with round leading edges is described. The flows include those at high subsonic and supersonic speeds about three wings, two of which are designed for attached flow at supersonic manoeuvre conditions. The main flow features on and off design are identified, including separations at the leading edge at subsonic speeds and at the shock at supersonic speeds. Scale effects on flows with leading-edge separation are described and means of simulating flight conditions for such flows by the use of transition trips are discussed. A method for solving Euler's equations is assessed by comparison with experiment and is shown to be inadequate for flows with separation. A technique for prescribing the flow conditions at shock-induced separation in an Euler solver is shown to give predictions in good agreement with measurement.

1 Introduction

The need for combat aircraft to operate effectively over a wide range of speeds means that the designer may have to accept compromises in the wing aerodynamic characteristics. For example, a wing fully optimised for supersonic manoeuvre may be unable to meet subsonic-flight requirements. Faced with this prospect, the designer is likely to select a wing having limited regions of separation at the supersonic manoeuvre condition. A similar compromise might have to be made with design for subsonic manoeuvre to ensure an adequate supersonic performance.

Design compromises can be minimised by the use of variable geometry to eliminate separation or to exploit separated flows, as with vortex flaps. However, variable geometry involves extra structural complexity and weight which could be minimised if the performance disadvantages (or advantages) of separated flows could be quantified. Unfortunately, Computational Fluid Dynamic (CFD) methods are not yet sufficiently mature to be used confidently to calculate flows with significant regions of separation on wings[1].

This paper describes a combined, experimental-theoretical study of flows over three highly-swept wings suitable for supersonic combat aircraft. The wings have round leading edges to ensure attached flow there for a wide range of supersonic-flow conditions, and two of the wings are cambered with the aim of ensuring weak shocks and attached flow on the upper surface at supersonic manoeuvre conditions.

The main aim has been to study flows over these wings to establish the effects of departures from the design condition at supersonic speeds as well as the flow characteristics of the wings at subsonic speeds. At subsonic manoeuvre conditions, flows near the leading edge of wings with round noses are characterised by rapid acceleration between the attachment line and the nose, followed by sharp retardation. The consequence of the latter can be separation, the nature of which depends on subtle features of the boundary layer near the leading edge, with the result that these flows can be sensitive to Reynolds number and to precise details of the leading-edge geometry; this further complicates the task of the designer by making it difficult to infer the characteristics of the full-scale aircraft from sub-scale tests in the wind tunnel, as is shown later. At supersonic speeds, separations may be induced by shocks on the wing upper surface.

A subsidiary aim has been to assess CFD methods by comparing predictions by them with measurement and, where necessary, to suggest possible changes to the modelling in the methods.

Between a description of the experiment in Section 2 and the Conclusions, the paper is divided into two parts. Section 3 deals with the study of flows at subsonic speeds while Section 4 is concerned with supersonic-speed flows. Subsonic-speed flows are considered first because they are more complex and challenging to understand than those at supersonic speeds. The scale effects on subsonic-speed flows over a wide range of Reynolds number and the prospects for simulating their features at high Reynolds number in sub-scale tests by the use of transition trips are discussed in Section 3.

2 Model and test details

The experiments were performed in the 8 ft x 8 ft Wind Tunnel at RAE Bedford on a series of three half models of wing-body combinations. All three wings were mounted on the same half body which was, in turn, supported from outside the working section. Following unpublished studies of half-model test techniques at RAE, the plane of symmetry of the model was displaced from the sidewall by an amount approximately equal to the wall boundary-layer displacement thickness, as illustrated in Fig 1. The wings all had the same delta planform of 60° leading-edge sweep and thickness distribution of 4% thickness-chord ratio. The leading-edge radius of streamwise sections was virtually constant across the wing span with a value 0.13% centre-line chord, c_o. Further details of the planform and thickness distribution can be found in Ref 2.

Details of the wing geometries are given in Fig 1. Two of the wings, A and B, were intended to have weak shocks and attached flow at lifting conditions representative of those for sustained manoeuvre at a free-stream Mach number, M_∞, of about 1.6. Wing A has a camber distribution based on that of a previous linear-theory design[3] suitable for a supersonic transport aircraft and shaped so that, according to linear theory, the attachment line is on the leading edge, ensuring attached flow there, at a lift coefficient of about 0.1 and $M_\infty = 1.5$. The 'design' lift coefficient is roughly a third of that needed for

sustained manoeuvre but subsequent experience, to be described in Section 4, shows that the flow remains attached for lift coefficients approaching the required value. The camber distribution is complex, the wing being cambered in both streamwise and spanwise directions.

Wing B was designed using the COREL full-potential code[4,5] (developed at Grumman Aerospace and made available to RAE by NASA under a collaboration between NASA and RAE) to have attached and shock-free flow on the upper surface at a lift coefficient of 0.3 and at a Mach number of 1.6. This wing has a conical camber distribution with its apex located at the junction of the wing leading edge and the body.

Finally, Wing C is uncambered and was included as a datum for the study of camber effects.

A photograph of one of the models is shown in Fig 2. With a centre-line chord of 1.8 m, the models are large, allowing the wings to be manufactured to high accuracy, permitting flow measurements and visualisations to be made in great detail and enabling tests to be performed at high Reynolds numbers.

The measurements made include:

i overall forces on the model (wing plus body) by means of a strain-gauge balance located outside the working section;

ii wing-surface static-pressures at about 300 holes, each of 0.5 mm diameter, drilled normal to the surface and distributed across the span at 9 axial stations (Fig 1);

iii oil-filament flows, obtained by pumping oil of three different colours onto the wing upper surface through small holes, as well as a limited number of conventional, surface oil-flows;

iv laser-illuminated vapour screens at supersonic speeds[2,6,7].

Tests at subsonic speeds were made for Mach numbers between 0.5 and 0.8 for Wings A and B and for 0.5 and 0.6 for Wing C, and for Reynolds numbers based on geometric mean chord $\bar{c}$ ($= 0.542c_o$), $R_{\bar{c}}$, between 6×10^6 and 29×10^6 (or, based on the leading-edge radius of streamwise sections, R_ρ, between 1.6×10^4 and 7×10^4). Measurements were also made for Mach numbers in the range 1.4 to 2 and for values of $R_{\bar{c}}$ up to 13×10^6, at which the main part of the tests at supersonic speeds was performed.

At subsonic speeds, tests were made with free transition on the wing upper surface and also with transition fixed by various trips placed, in turn, near the leading edge with the aim of provoking transition on the upper surface. These include a trip with its front edge on the wing leading edge ('leading-edge' trip) and another on the upper surface 2.5 mm from the leading edge in plan view ('upper-surface' trip). The trips consisted of bands of sparsely-distributed ballotini (glass spheres) cemented by epoxy resin onto the wing along a strip 5.1 mm wide. Strictly, the trip height needed to fix transition depends on Reynolds number and local Mach number. However, to economise on tunnel run time, only one grade of ballotini, in the range of diameters 0.21 mm to 0.25 mm, was used for the above-mentioned trips. This grade was determined[8] by the need to fix transition at the lowest Reynolds number and highest expected local Mach number of the tests at subsonic speeds. For the main part of the tests at supersonic speeds at $R_{\bar{c}} = 13 \times 10^6$, a trip (also of 5.1 mm width but with ballotini of diameter in the range 0.25 mm to 0.3 mm) was placed on the upper surface 25.4 mm from the leading edge in plan view, and, at all speeds, an identical trip was placed at the same position on the lower surface.

Corrections have been applied to the force data at subsonic speeds for blockage[9] and for lift interference[10] and to the pressure data for blockage. No tunnel-wall corrections were necessary for tests at supersonic speeds. No corrections were made to model angle of incidence for aeroelastic distortion since these were believed to be negligible.

3 Subsonic-speed flows

3.1 Cambered wings

The two cambered wings were found to have similar flow characteristics at subsonic speeds and so only data for Wing A are discussed here.

a. Free transition

Data for overall forces, typical of all those for subsonic speeds, are shown in Fig 3 for $M_\infty = 0.6$ and for the two extremes of the test Reynolds-number range, data for intermediate Reynolds numbers having been omitted for clarity. The lift and pitching-moment curves are not affected greatly by Reynolds number but lift-dependent drag is scale sensitive for lift coefficients above about 0.4. The associated changes in flow are likely to have implications for other aspects of aircraft performance, eg lateral stability.

A better understanding of scale effects can be obtained by studying surface pressure distributions. Figs 4 and 5 illustrate the different character of the effects depending on whether the flow is attached or separated. Data for attached flows at an angle of incidence, $\alpha = 7.5°$ ($C_L = 0.2$) are shown in Fig 4 as spanwise pressure distributions (pressure coefficient, C_p, plotted against the ratio of spanwise distance from the model centre line to local wing semi-span, η) for a selection of the nine pressure runs. Since the scale effects are small, only data for the highest and lowest Reynolds number are shown. Also included are corresponding distributions calculated by a CFD code for solving Euler's equations for flows around complex configurations[11,12]. The agreement between inviscid calculation and measurement at both Reynolds numbers is reasonable, suggesting that boundary-layer displacement effects are small.

A completely different result is found at angles of incidence above about 10° where leading-edge separation is known to occur, as shown in Fig 5 for $\alpha = 11.7°$, $C_L = 0.48$. In this case, the

agreement between inviscid calculation and measurement is much poorer on the upper surface, as might be expected, particularly at the lowest Reynolds number. Furthermore, scale effects are significant for Reynolds numbers up to the maximum and are particularly marked between $R_{\bar{c}} = 6 \times 10^6$ and 19×10^6. The accurate calculation of flows of this type appears beyond our means at present because of the lack of reliable turbulence and transition models[1].

Scale effects similar to those in Fig 5 were found at comparable lift coefficients for other Mach numbers in the range 0.5 to 0.8 and also in pressure measurements made in flight at a streamwise section of the wing of an F-111 TACT aircraft[13]. Poll[14] noted that the Reynolds numbers based on the section leading-edge radius for these flight tests, which he estimated to be $R_\rho = 5 \times 10^4$ and 10^5, are within the critical region for changes to occur in the boundary layer near the leading edge by three-dimensional transition. As noted before, the range of values of R_ρ for the present study is 1.6×10^4 to 7×10^4.

The scale effects shown in Fig 5 can perhaps be appreciated better by studying flows on the wing upper-surface for the two extremes of the Reynolds-number range, typical of conditions, respectively, for $R_{\bar{c}} \approx 6 \times 10^6$ and $R_{\bar{c}} > 19 \times 10^6$. Fig 6 shows isobars and sketched interpretations of surface oil-flows for these two cases. At $R_{\bar{c}} = 6 \times 10^6$, the isobars suggest that the flow is locally of a conical character with a well-developed vortex flow fed by a separation from the leading edge which originates from the point 'B'. This observation is confirmed by the corresponding oil flow which shows the characteristic outflow in the boundary layer beneath the vortex and the separation of this secondary boundary-layer in the region of rising pressure between the vortex and the leading edge. Sutton[15] argued that the shear layers from both the primary and secondary separations join together to feed the vortex and to enclose a bubble[16] (Fig 7a). At $R_{\bar{c}} = 29 \times 10^6$, the isobars are densely packed about a line that is roughly parallel to the leading edge downstream of the point 'B', suggesting a flow with a tendendy towards cylindrical rather than conical symmetry. The oil flows, on the other hand, indicate a more complex flow. Upstream of the point 'B', the oil runs along and from the leading edge and this, together with the pressure distributions in this region, suggests a 'short' bubble separation; further downstream, a series of disturbances shed from the leading edge at positions close to the pressure-measuring stations appear to influence the secondary boundary-layer in a region of vortical flow. Previous experiments[17,18,19] have shown that certain separated flows are sensitive to small surface imperfections upstream of the separation line. Although all three wings were manufactured to a high standard of surface finish, static pressure holes (the tubes to which were sealed) and minute gaps between cover plates could have been sufficient to cause disturbances near the leading edge where the boundary layer is extremely thin. This suggests that the isobar plot for $R_{\bar{c}} = 29 \times 10^6$ should be viewed with some caution because it is based on pressure measurements made at the origin of the disturbances which could themselves have influenced the pressures. The possibility also has to be considered that the disturbances may have controlled the flow and contributed to the scale effects. The disturbances extend along the leading edge from the point 'B' to a point at about 80% chord, downstream of which there is a vortex type flow with a region of secondary separation. The exclusiveness of these two regions is also evident in the oil-flow studies of Ref 17. The position where the bubble bursts, 'B', corresponds with a marked reduction of the leading-edge suction peak with distance along the leading edge, and, despite the large scale effects on the flow, this position changes slowly with Reynolds number.

There would appear to be two main clues to the causes of the observed scale effects. The first is the 'short' bubble which is inferred from the oil flow at the highest Reynolds number (Fig 6), suggesting that the flow at the leading edge is not fully turbulent over the range of Reynolds numbers studied. To assess the likelihood of this, calculations have been made using criteria for attachment-line transition[20] and relaminarisation[21] along with measured and predicted surface-pressure distributions to infer the velocity distribution at the outer edge of the boundary layer (the external flow). The criterion for the attachment line to become turbulent due to contamination from the body boundary layer is given by[20]:

$$\bar{R} = V\zeta/\nu > 300 ,$$

where

$$\zeta = \sqrt{\nu/(dU/ds)_A} ,$$

V and U are the components of external-flow velocity, Q , along the attachment line and in the plane normal to the attachment line, and s is the distance along the wing surface in the same plane. Suffix A refers to the attachment line. A parameter which has been suggested[21] for determining the prospects for relaminarisation is:

$$K = \{\nu/Q^2\} dQ/d\sigma ,$$

where σ is distance along the external-flow streamline. It is supposed that the velocity component V does not vary around the leading edge at each section and is determined by conditions at the attachment-line, assumed to correspond to the local maximum in pressure. In Ref 21 it is stated that, for the flow to revert completely to laminar form, K must exceed 5×10^{-6} but that a departure from fully-turbulent flow (or incomplete relaminarisation) may take place for values greater than 2×10^{-6}. The relaminarisation criteria are based on studies of two-dimensional boundary layers and so should perhaps be treated with some caution. Moreover, both criteria necessitate the determination of gradients with, inevitably, some uncertainty about the accuracy of the estimates. Fig 8a shows axial variations of $\bar{R}$ and the peak value of K , or K_{max} , for $\alpha = 11.7°$ and $R_{\bar{c}} = 6.4 \times 10^6$. Given this uncertainty, the agreement between the estimates made using measurements and Euler predictions of

surface pressures may be considered reasonable, and this is due to the respective pressure distributions being in relatively good agreement where the parameters are evaluated. This suggests that inviscid CFD methods may be used to predict boundary-layer conditions in the attached-flow region near the leading edge, and may therefore be used to decide a strategy for simulating leading-edge boundary-layer states ahead of tunnel tests. Boundaries in the (α , $R_{\bar{c}}$) plane for attachment-line transition and subsequent relaminarisation, determined from measured pressure distributions, are illustrated in Fig 8b for a typical axial station. This figure shows that the attachment line is likely to be fully turbulent at α = 11.7° over the range of test Reynolds numbers. It indicates that relaminarisation is complete at this angle of incidence for values of $R_{\bar{c}}$ below about 13 x 10^6 (R_ρ<3 x 10^4) and is incomplete (so that the boundary layer is neither laminar nor turbulent) for higher values up to $R_{\bar{c}}$ = 38 x 10^6. This suggests that the leading-edge flow is not turbulent* even at the highest Reynolds number of the tests and that correct simulation of flows at higher Reynolds number probably requires a transition trip close to the leading edge (see later).

The second clue is the secondary separation at $R_{\bar{c}}$ = 6 x 10^6. Smith[22] showed that, for thin shear layers embedded in an irrotational, isentropic flow, a separated vortex sheet leaves a smooth surface tangentially, as sketched in Fig 7b, to ensure that vorticity is shed at separation. However, this flow model excludes bubbles, and visualisations of the flow over a body by Costis et al[23] suggest that, where secondary separation occurs, the primary vortex sheet separates from the body surface at a non-zero angle (Fig 7a). Thus, for a fixed primary-separation line, the onset of secondary separation may be expected to cause a reduction in flow velocity normal to and just upstream of this line, leading to an increase in pressure in this region. This is consistent with observations of the present study which are best illustrated by pressure distributions around the leading edge, as shown for two axial stations in Fig 9. Judging by these data, the primary separation line does not change position much with Reynolds number. However, the pressures in this region increase significantly between high and low Reynolds number, ie between flows, respectively, largely without and with secondary separations. Accompanying this change, is an increase in the area of the wing affected by the separation which may be related to the same phenomenon. Fig 9 also shows that the pressure gradients between the suction peak and the leading edge are milder at $R_{\bar{c}}$ = 6.4 x 10^6 than at $R_{\bar{c}}$>19 x 10^6, suggesting that the secondary boundary-layer is laminar at the lower Reynolds number. This points to the possibility of tripping the secondary boundary-layer at low Reynolds number to simulate the conditions beneath the main vortex at higher Reynolds numbers, a prospect that is discussed later. Evidence from tests on slender delta wings[24] shows that a change from laminar to turbulent conditions in the secondary boundary-layer results in increased peak suction although, for such wings, the secondary separation is distinct from the primary separation. Haines[25] showed that, for a wing of 50° quarter-chord sweep, a fence placed part-way across the span located a vigorous vortex separation, the outflow under which moved the secondary separation further outboard than it would otherwise have been, possibly because the new, secondary boundary-layer was thinner and less prone to separation than that without the fence.

*It is possible that the relaminarised flow reverts to turbulent conditions but, at present, methods are only available for predicting transition in flows that are wholly laminar further upstream.

b. Upper-surface transition trips

Fig 10 shows pressure distributions for the case considered previously (M_∞ = 0.6, α = 11.7°) but with the 'leading-edge' trip. Calculations referred to above show that this trip is downstream of where relaminarisation is expected. In contrast with the free-transition case, the pressure distributions are insensitive to Reynolds number and are in better agreement with predictions by the Euler method than before except possibly at the most-aft measuring station. The relative lack of scale effects in this case may be taken as indirect evidence that the scale effects for the free-transition case arise in part from the boundary layer at the leading edge being laminar or not fully turbulent, in agreement with the calculations illustrated in Fig 8b.

The influence of different trips on pressure distributions around the leading-edge at two axial stations is shown in Fig 11. Three sets of data are included: 'leading-edge' and 'upper surface' trips for $R_{\bar{c}}$ = 13 x 10^6 and free transition at $R_{\bar{c}}$ = 29 x 10^6. Also included for comparison are the pressure distributions calculated by the Euler code. The 'leading-edge' trip is seen to give higher peak-suctions and to have a pressure distribution of different shape to that for free transition. It is possible that the 'leading-edge' trip simulates a flow with free transition at an even higher Reynolds number, as implied in Fig 8b. On the other hand, Fig 11 indicates that a leading-edge trip would give misleading data were it to be used in low Reynolds-number tests to simulate conditions at values of $R_{\bar{c}}$ up to about 30 x 10^6. It is also possible that the 'leading-edge' trip influences the external flow since its height is a significant proportion of the leading-edge radius and it is closer to the suction peak than is perhaps desirable[26].

Figs 11 and 12 show that a closer simulation of the free transition flow at the highest Reynolds number is obtained by the use of the 'upper-surface' trip at $R_{\bar{c}}$ = 13 x 10^6 (corresponding to the maximum Reynolds number achievable with a complete model in the 8 ft x 8 ft Tunnel). This simulation is achieved despite the fact that this trip is slightly inboard of the leading-edge suction peak (Fig 11). It is speculated that the 'upper-surface' trip provokes transition of the secondary boundary-layer so that the flow beneath the vortex is similar to that occurring naturally at the higher Reynolds number. On the other hand, the 'upper-surface' trip was not successful in simulating high Reynolds-number conditions at the lowest Reynolds number, possibly because it was not sufficiently far inboard to influence the

secondary boundary-layer. This suggests that a trip placed further inboard may have been more suitable in this respect.

3.2 Symmetrical wing

As with the cambered wings, lift and pitching moment of Wing C are not greatly affected by changes in Reynolds number, as shown in Fig 3 for the free-transition case and $M_\infty = 0.6$.

Features of the flows over Wing C that are worthy of note are illustrated in Fig 13 which shows pressures distributions around the leading edge at two axial stations for $M_\infty = 0.6$ and $\alpha = 7°$ ($C_L = 0.35$). According to calculations by the Euler code, this case has minimum values of pressure coefficient of roughly the same magnitude as those for the cambered wing case at $\alpha = 11.7°$. For the free-transition case (Fig 13a), the leading-edge suctions at $R_{\bar{c}} = 6 \times 10^6$ are significantly lower than those at higher Reynolds number, as noted for Wing A. On the other hand, at the highest Reynolds number, the adverse-pressure gradients in this region are larger than those for Wing A (see Fig 9), suggesting a change in the character of the boundary layer at primary separation between the wings. This view is supported by calculations of the relaminarisation parameter for Wing C which show that, at the highest Reynolds number, K_{max} is just greater than 2×10^{-6} at Station 6 ($x/c_o = 0.705$), corresponding to the upper bound for fully-turbulent flow, whereas, for Wing A at the same station and at $R_{\bar{c}} = 29 \times 10^6$, $K_{max} = 2.8 \times 10^{-6}$. Scale effects are small when the 'leading-edge' trip is fitted (Fig 13b), as before, but, by contrast, the effect of the trip is to increase the extent of the separated flow over the wing compared with that for free transition at high Reynolds number. This is the opposite of what was found with the cambered wings and is similar to the result obtained in a flight-tunnel comparison of flows over the wing of a Fairey Delta 2 aircraft[27] which also has a symmetrical wing of 60° leading-edge sweep. The tunnel tests were made with the boundary layer tripped by a roughness band placed around the leading edge, whereas, in flight, transition to turbulence in the boundary layer took place naturally. Despite the flight and tunnel Reynolds numbers not differing greatly, the tunnel tests show a larger area of the wing upper surface affected by separation for a given angle of incidence than do the flight tests.

It is possible that, in both tunnel tests, the boundary layer was unduly thickened as a result of the trip being downstream of the suction peak (Fig 13) with the consequence that the trip caused premature separation. Taken together, these results show the need to treat data with trips on the leading edge with caution and to perform supplementary tests with natural transition to aid the understanding of the flows[26].

4 Supersonic-speed flows

Although supersonic combat aircraft have been in operation for some time, it has only recently become possible to calculate accurately the transonic flows found above the wings at supersonic manoeuvre. The opportunities for designing supersonic wings with transonic flows were probably first pointed out by Mason and Daforno[28]. Following this suggestion, a conical wing was designed using the conical full-potential code COREL, referred to before, to have shock-free attached flow at a typical manoeuvre condition, and subsequent tunnel tests showed that the design was successful[29].

Perhaps inspired by this success, Grumman developed a non-conical variant of COREL known at NCOREL[30]. This method uses a streamwise space marching technique and is thus limited to wholly supersonic flows. A non-conical wing was designed by the new method to have shock-free attached flow at relatively-high lift and, again, tunnel tests showed that the design objectives were achieved[31].

The emphasis in UK has been on the development of methods for solving the Euler equations using time stepping to achieve a steady-state solution. As well as allowing calculations over complex configurations, the Euler code, referred to in Section 3, ensures a more accurate simulation of the changes in flow quantities across shock waves than is possible with full-potential methods and it can be used for predictions over the complete speed range. As noted in the Introduction, one of the aims of the study has been to assess CFD methods as design tools, and data obtained from the tests have been used for this purpose as well as for identifying the main flow features.

4.1 Assessment of CFD and main flow features

Fig 14 illustrates a typical set of data used to interpret the flows for Wing A at $M_\infty = 1.6$, typical of a sustained manoeuvre condition, and for three lift coefficients (0.2, 0.3 and 0.4). The pressure measurements (upper-surface isobars), oil-filament flows and laser-illuminated vapour screens are in agreement in showing the effects on the flow of a shock above the wing upper surface at all three conditions and indicating separation at the foot of the shock for $C_L = 0.3$ and 0.4. The data shown in Fig 14 and in the rest of the section are for $R_{\bar{c}} = 13 \times 10^6$ but measurements made on Wing B at Reynolds numbers down to 3×10^6 (also with transition fixed near the leading edge) suggest that scale effects on these flows are small in the range $R_{\bar{c}} = 3 \times 10^6$ to 13×10^6.

Comparisons between calculated and measured pressure distributions for all three wings at given angles of incidence are shown in Fig 15 for $M_\infty = 1.6$ and three approximate lift coefficients. The pressure distributions for $C_L \approx 0.2$ (Fig 15a) show that the flow expands gradually around the leading edge on Wing A and that, on Wing B, the suctions on the outer 5-10% span on the upper surface are higher than those on Wing A; they also reveal that there is a re-expansion of the flow on the upper surface of Wing B. Wing C has the highest suctions near the leading edge on the upper surface of all three wings, with some isentropic recompression upstream of the shock. The agreement between prediction and measurement is satisfactory, except possibly just inboard of the shock where boundary-layer displacement effects are likely to be more severe than elsewhere. The impressive feature of the comparison is the ability of the method to predict three different flows with weak shocks. In this respect, the method is

expected to be useful for the design of supersonic transport aircraft as well as of combat aircraft.

At angles of incidence corresponding to the higher lift coefficient 0.3 (Fig 15b), which is close to that needed for sustained manoeuvre, the agreement between prediction and measurement is reasonable overall except inboard of the shock on Wings A and B where, as in indicated in the measured pressure distributions and in flow visualisations (see Fig 14 for Wing A), there are clear signs of shock-induced separation.

For a lift coefficient of 0.4 (Fig 15c), shock-induced separation is evident on all three wings and, as at the lower lift coefficient, the Euler method, lacking the modelling of viscous effects, is unable to represent this feature. In all the cases of Fig 15, the flow at the leading edge is attached, except possibly aft of 90% chord on Wing C at $C_L \simeq 0.4$ showing that the main concern with flows at supersonic manoeuvre conditions is shock-induced separation. For design studies, where trade-offs need to be considered between supersonic and subsonic performance, it would be useful to be able to predict accurately flows of this type. Some progress has been made by Kwong and Myring[32] in the calculation of flows over missile bodies using an Euler solver combined with the 'forced separation' approach in which the flow is forced to separate at a non-zero angle relative to the wing surface at the foot of the shock (see Fig 16). Marconi[33] argued that separation at a non-zero angle is consistent with Smith's conception of separation[22] because, in this case, the component of the external flow normal to and just upstream of the separation line is not at rest and so vorticity is shed at separation. The boundary layers are assumed to be thin and only to enter the calculation through the determination of the position of separation. This process is performed interactively with the inviscid-flow calculation which makes use of an empirically-derived deflection angle at the foot of the shock. Inclusion of this model of separation was shown to give improved agreement with experiments[32].

4.2 Modelling of shock-induced separation

A similar approach could be used for wings. However, wing flows are likely to be more sensitive to errors in the modelling than are flows over missiles and, for wings, it is probably necessary to model the flow deflection at the separation line more accurately than for missile bodies. A method for determining this deflection angle is described below.

To isolate the assessment of the method from any inaccuracies in the Euler solver, the boundary layer upstream of the shock is calculated using the measured pressure distribution upstream of the shock. Since there is insufficient detail in the measured pressures in the region of the shock, the shock is treated as a sudden rise in pressure, its position being determined from measured pressures in the way shown in Fig 16. Following Kwong and Myring, the boundary layer upstream of separation is assumed to be 'thin' so that the assumptions of boundary-layer theory apply.

The boundary layer is calculated to the point 'a' just upstream of the shock using a method for conical flows with adiabatic wall conditions. This method is based on a technique for tapered wings[34] and its use is justified by the conical nature of supersonic flows over delta wings. Boundary-layer transition is taken at the leading edge of the transition trip. Since the surface pressure is assumed to rise suddenly at the shock, the boundary layer development within the shock is calculated using another variant of the tapered-wing method in which shear stresses are ignored. In this calculation, the initial conditions at the point 'a' of the boundary layer parameters and the external-flow conditions are, respectively, given by those from the conical-flow method and are inferred from the measured pressures using the isentropic-flow relationships (the use of which is justified in this region for free-stream Mach numbers of interest, ie up to 2), the measured sweep-angle of the shock and the assumption that, locally, the flow is of the infinite swept-wing type. From the latter conditions, it is possible to calculate M_a, the Mach number of the external-flow component normal to the shock at 'a' in the plane tangential to the wing surface at 'a' (the tangent plane).

Both boundary-layer methods use the assumption of isentropic flow to determine the density of the external flow. As noted above, this assumption can be justified upstream of the shock but, for the calculation of the boundary layer within the shock, further justification is needed and this will be offered later.

The calculation is taken to the point 'b' where separation occurs, ie where the streamlines limitingly close to the wing surface converge on a line just inboard of the locus of the shock on the wing surface (Fig 16); at this point, the Mach number of the external-flow component normal to the shock in the tangent plane, M_b, is determined. Knowing the two Mach numbers M_a and M_b, it is possible to determine the flow deflection angle θ and the associated shock inclination β using the theory of oblique shock waves[35]. To assess these predictions, measurements have been made of the two angles from photographs of laser-illuminated vapour screens above Wing A taken by a camera in a pod to the rear of the model. Fig 17 shows comparisons of calculations by the present method and averaged values of a number of measurements of shock inclination and flow deflection against the Mach number M_a. In both cases, the present method reproduces the observed trends and gives values which are close to measurement. Also shown are the angles corresponding to maximum deflection of the flow through an oblique shock. Fig 17 reveals that, as M_a increases, the inclination of the shock decreases so that the shock strength, $M_a \sin\beta$ remains roughly constant at about 1.2. For a Rankine-Hugoniot shock, the associated density ratio is 1.342, whereas for an isentropic shock with the same values of M_a and M_b the density ratio is 1.351. Since the difference between the two ratios is small, the errors resulting from the use of the isentropic-flow relationship in the boundary-layer calculation through the shock are expected to be small.

The use of this method or a variant of it within an interactive scheme, using an Euler

solver with forced separation to determine the pressure distribution, remains a task for the future but these comparisons suggest that it is worthwhile to make the necessary modifications to Euler methods.

5 Conclusions

The emphasis of the first part of the study has been on scale-sensitive features of flows at subsonic speeds with leading-edge separation. These flows, unlike attached flows, are not adequately modelled by current CFD methods and so their characteristics at flight conditions have to be determined by wind-tunnel test. A superficial study of overall forces and pitching moment would suggest that scale effects on separated flows are insignificant but a detailed examination of flows shows that this is not the case. This conclusion applies to all three wings over the range of Mach numbers studied (between 0.5 and 0.8 for the cambered wings) but further conclusions are based mainly on a study of separated flows over cambered Wing A at $M_\infty = 0.6$ and $\alpha = 11.7°$ ($C_L = 0.48$) and are as follows:

1 With free transition on the wing upper surface, the flows are scale sensitive for values of $R_{\bar{c}}$ up to about 19×10^6 ($R_\rho = 4.7 \times 10^4$). At $R_{\bar{c}} = 6 \times 10^6$ ($R_\rho = 1.6 \times 10^4$) the flow above the wing is locally of conical character with a main vortex and a secondary separation. At $R_{\bar{c}} = 19 \times 10^6$ and above the flow exhibits a series of small disturbances shed from the leading edge at positions close to the pressure-measuring stations. This region terminates at about 80% chord, downstream of which there is a vortex flow with a secondary separation.

2 A transition trip placed on the leading edge gives surface pressure distributions that are much less scale sensitive than those with natural transition. However, these distributions differ significantly from those with free transition at the highest Reynolds number of the test ($R_{\bar{c}} = 30 \times 10^6$). This was also found to hold for the symmetrical wing at the same Mach number except that, by contrast with Wing A, the trip increased the region of separated flow above the wing compared with that for free transition at high Reynolds number.

3 A satisfactory simulation of a flow with free transition at $R_{\bar{c}} = 29 \times 10^6$ was achieved at $R_{\bar{c}} = 13 \times 10^6$, corresponding to the maximum for a complete model in the RAE 8 ft x 8 ft Wind Tunnel, by using a trip placed inboard of the leading-edge suction peak on the upper surface.

Conclusions 1 and 2 show, respectively, the complexity of scale effects on flows with leading-edge separation and the difficulty of simulating their features at high Reynolds number in subscale tests. Following recommendations in Ref 26, calculations should be made ahead of the tests to establish the flow conditions to be simulated in the leading-edge region. This can be done using an attached flow CFD method. If this flow is laminar or transitional, a trip upstream of the primary separation line is inappropriate. If, on the other hand, the flow is turbulent, results from tests with leading-edge trips should be examined to determine if the trip has affected the flow in any way. In some cases, it may be of greater importance to simulate flight conditions in the secondary boundary-layer beneath the main vortex. For example, if this boundary layer is laminar in the test and is expected to be turbulent in flight, a trip should be placed between the reattachment line and the recompression region further outboard.

The main conclusions of the study at supersonic speeds (for a Mach number typical of a sustained manoeuvre condition, 1.6, and at $R_{\bar{c}} = 13 \times 10^6$) are as follows:

1 An Euler CFD code for calculating inviscid flows over complex configurations gives satisfactory predictions of wing-surface, pressure distributions for attached flows and may therefore be used to design wings with weak shocks for sustained manoeuvre at supersonic speeds.

2 A simple model of shock-induced separation represents the main features of the flow at separation and may be used as the basis for the viscous element of a 'forced separation' Euler method.

The investigation as a whole has highlighted features of separated flows over highly swept wings with round leading edges, and has shown how these flows may be predicted either from wind-tunnel tests or by adapting existing CFD methods.

Acknowledgements

The authors would like to thank Mr G L Riddle, Mrs I Gaudet and Mrs N Rycroft for their efforts in preparing the diagrams.

References

1 P-M Hartwick, C-H Hau, J M Luckring, C H Liu; 'Aerodynamic applications of an efficient incompressible Navier-Stokes solver'. ICAS-88-5.9.1, (1988)

2 P R Ashill, J L Fulker, M J Simmons; 'A study of flows over highly-swept wings designed for manoeuvre at supersonic speeds' Royal Aero. Soc. Symposium 'Aerodynamic design for supersonic flight' 19 April 1988

3 J H B Smith, J A Beasley, Diana Short, F Walkden; 'The calculation of the warp to produce a given load and the pressure due to a given thickness on thin slender wings in supersonic flow'. ARC R&M 3471 (1967)

4 B. Grossman; 'Numerical procedure for the computation of irrotational flows'. AIAA Journal, Vol 17, 8, pp 828-837 (1979)

5 W H Mason, B S Rosen; 'The COREL and W12SC3 computer programs for supersonic wing design analysis' NASA CR 3676 (1983)

6 I McGregor; 'The vapour screen method of flow visualisation' *Journal of Fluid Mechanics* Vol 11, 4, pp 481-511 (1961)

7 L Gaudet, M N Cripps; 'A scheme for a laser-illuminated vapour screen flow visualisation technique for the RAE 8 ft x 8 ft Wind Tunnel' RAE unpublished

8 J Y G Evans; 'Transition fixing techniques and the interpretation of boundary layer conditions on slender wings in supersonic wind tunnels' RAE TN Aero 2946 (1964)

9 D Isaacs; 'Calibration of the RAE Bedford 8 ft x 8 ft Wind Tunnel at subsonic speeds, including a discussion of the correction to the measured pressure distributions to allow for the direct and blockage effects due to the calibration probe' ARC R&M 3583 (1969)

10 W E A Acum; 'Correction for symmetrical swept and tapered wings in rectangular wind tunnels' AEC R&M 2777 (1950)

11 R H Doe, A Pagano, T W Brown; 'The development of practical Euler methods for aerodynamic design' ICAS-86-5.5 (1986)

12 N P Weatherill, C R Forsey; 'Grid generation and flow calculations for aircraft geometries' J. Aircraft, Vol 22, 10, pp 855-860 (1985)

13 J E Lamar, J F Campbell; 'Recent studies at NASA Langley of vortical flows interacting with neighbouring surfaces' Paper 10, AGARD-CP-342, 'Aerodynamics of vortical type flows in three dimensions' (1983)

14 D I A Poll; comment in 'Round table discussion' AGARD-CP-342, 'Aerodynamics of vortical type flows in three dimensions' (1983)

15 E P Sutton; 'Some observations of the flow over a delta-winged model with 55-deg leading-edge sweep, at Mach numbers between 0.4 and 1.8' ARC R&M 3190 (1960)

16 E C Maskell; 'Flow separation in three dimensions' ARC 18063 (1955)

17 F O'Hara, J B Scott-Wilson; 'An investigation of the flow over a half-wing model with 60.5° leading edge sweepback, at a high subsonic and supersonic speeds' ARC CP 471 (1955)

18 E P Sutton; 'Experiments on a flow with swept separation and reattachment of a boundary layer' Proceedings of IUTAM Symposium 'Three-dimensional turbulent boundary layers', Berlin, March 1982, Springer-Verlag

19 D I A Poll; 'On the generation and subsequent development of spiral vortex flow over a swept-back wing' Paper 6, AGARD-CP-342 'Aerodynamics of vortical type flows in three dimensions' (1983)

20 D I A Poll; 'Transition in the infinite swept attachment line' Aero Quart Vol 30, 4, pp 607-629 (1979)

21 M G Hall, D A Treadgold; 'Difficulties in predicting boundary-layer transition on swept wings' Paper 2, AGARD-R-602 'Fluid motion problems in wind tunnel design' (1973)

22 J H B Smith; 'Behaviour of a vortex sheet separating from a smooth surface' RAE TR 77058 (1977)

23 C E Costis, N T Hoang, D P Telionis; 'Laminar flow over a prolate spheroid' J. Aircraft, Vol 26, 9, pp 810-816 (1989)

24 J H B Smith, A G Kurn; 'Pressure measurements on a slender rhombic cone at incidence at Mach numbers from 0.4 to 1.1' ARC R&M 3626 (1970)

25 A B Haines; 'Some notes on the flow patterns observed over various sweptback wings at low Mach numbers (in the RAE 10 ft x 7 ft High Speed Tunnel)' ARC R&M 3192 (1960)

26 A B Haines; 'Combat aircraft' Section 3.2.1 AGARD-AR-224 'Boundary layer simulation and control in wind tunnels' (1988)

27 F W Dee, O P Nicholas; 'Flight determination of wing flow patterns and buffet boundaries for the Fairey Delta 2 aircraft at Mach numbers between 0.4 and 1.3, and comparison with wind tunnel results' ARC R&M 3482 (1967)

28 W H Mason, G Daforno; 'Opportunities for supersonic performance gains through non-linear aerodynamics' AIAA-79-1527 (1979)

29 David S Miller, Emma Jean Landrum, James C Townsend, William H Mason; 'Pressure and force data for a flat wing and a warped conical wing having a shockless recompression at M = 1.62' NASA TP 1759 (1981)

30 M J Siclari; 'The NCOREL computer program for 3D non linear supersonic potential flow computations' NASA CR 3694 (1983)

31 W H Mason, M J Siclari, D S Miller, J L Pittman; 'A supersonic manoeuver wing designed for non linear attached flow' AIAA-83-0425 (1983)

32 C N Kwong, D F Myring; 'Fusiform body separated flowfield calculation using Euler and boundary layer methods' Royal Aero. Soc. Conference 'The prediction and exploitation of separated flow' 18-20 April 1989

33 F Marconi; 'Conical, separated flows with shock and shed vorticity' AIAA Journal Vol 25, 1, pp 173-175 (1987)

34 P R Ashill, P D Smith; 'An integral method for calculating the effects on turbulent boundary-layer development of sweep and taper' The Aeronautical Journal Vol 89, 882, pp 45-51 Feb 1985

35 H W Liepman, A Roshko; *'Elements of gasdynamics'* John Wiley & Sons (1957)

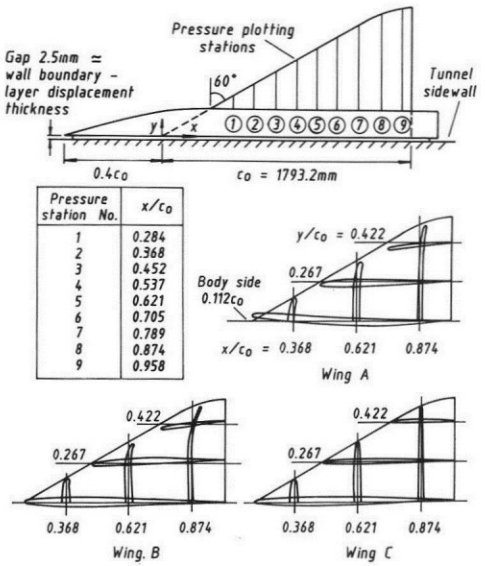

Fig. 1 Geometry of half model and wings.

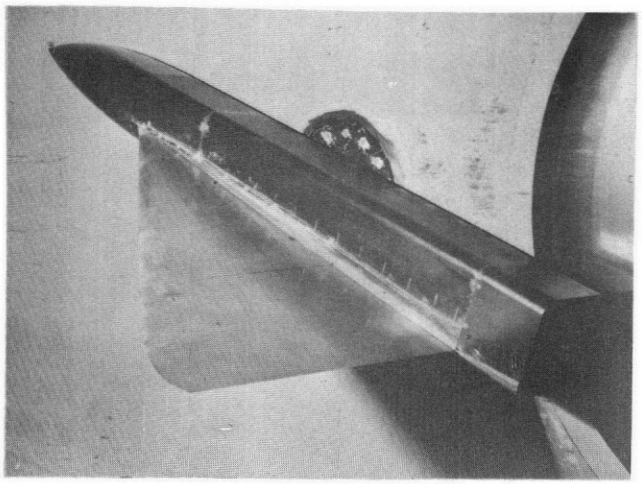

Fig. 2 Model mounted in tunnel.

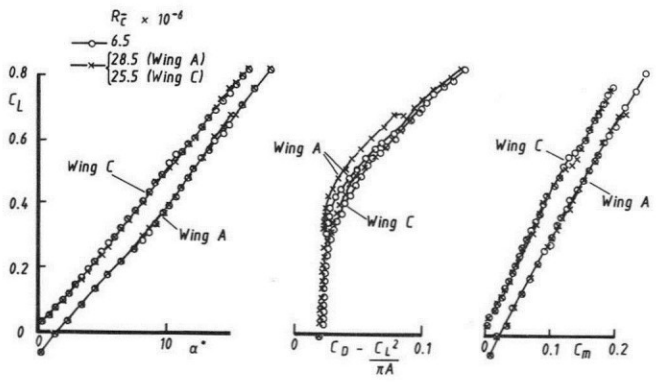

Fig. 3 Effects of Reynolds number on overall forces and pitching moment, free transition, $M_\infty = 0.6$.

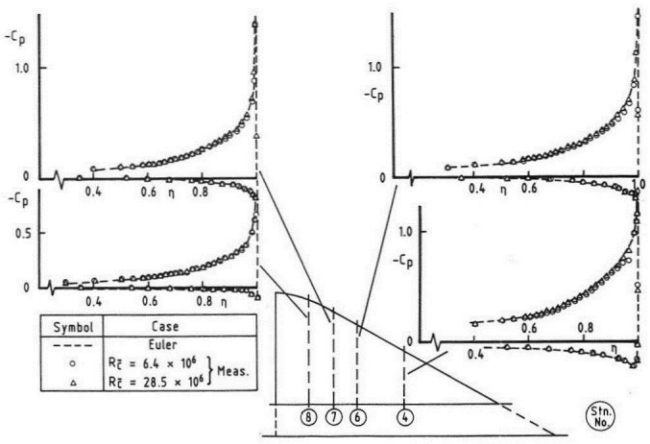

Fig. 4 Effect of Reynolds number on pressure distributions, Wing A, free transition, $M_\infty = 0.6$, $\alpha = 7.5^o$, $C_L = 0.21$.

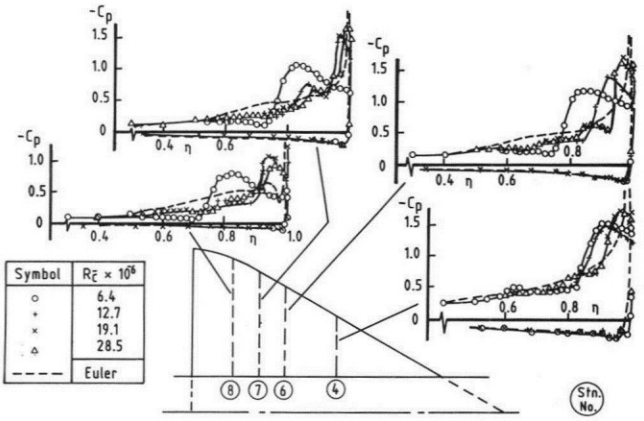

Fig. 5 Effect of Reynolds number on pressure distributions, Wing A, free transition, $M_\infty = 0.6$, $\alpha = 11.7^o$, $C_L = 0.48$.

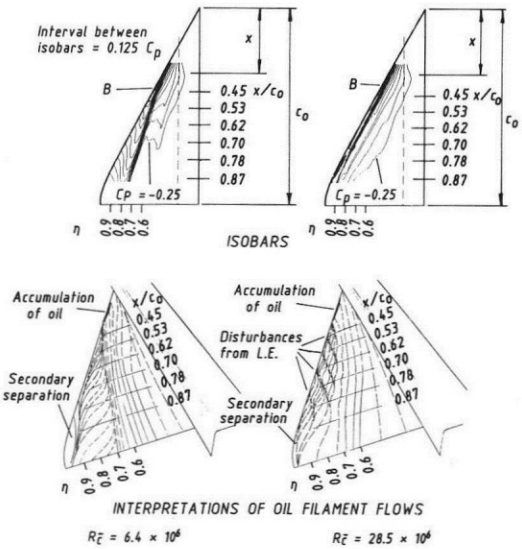

Fig. 6 Isobars and interpretation of oil flows, Wing A, free transition, $M_\infty = 0.6$, $\alpha = 11.7^o$.

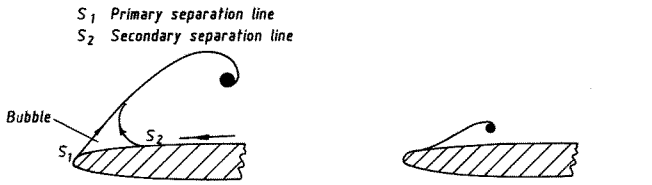

(a) Flow with secondary separation, Sutton [15], Costis et al [23]

(b) Smith's conception[22] of separation from a smooth surface

Fig. 7 Flow separation models showing spanwise cross-sections of stream surfaces.

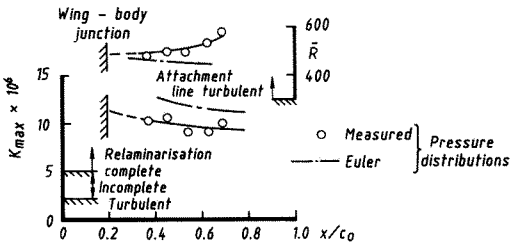

(a) Axial variations of attachment-line contamination and relaminarisation parameters, $\alpha = 11.7°$, $R_{\bar{c}} = 6.4 \times 10^6$

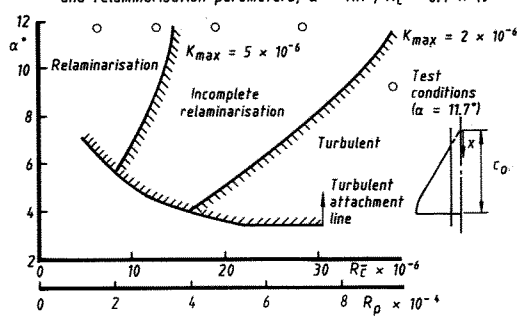

(b) Attachment-line contamination and relaminarisation boundaries, $x/c_0 = 0.705$

Fig. 8 Calculated attachment-line and leading-edge relaminarisation conditions, Wing A, $M_\infty = 0.6$.

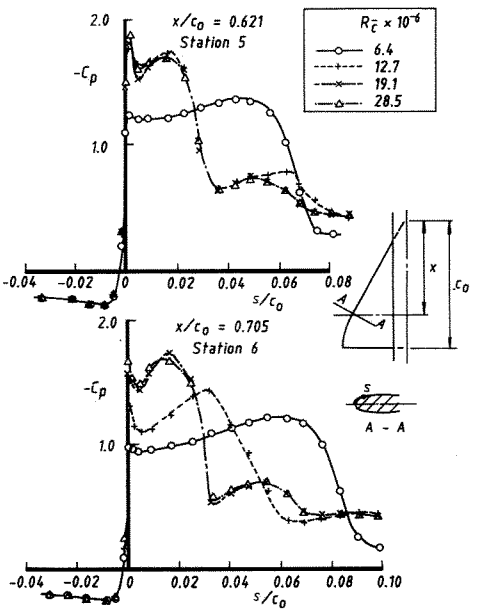

Fig. 9 Pressure distributions around leading edge, Wing A, free transition, $M_\infty = 0.6$, $\alpha = 11.7°$.

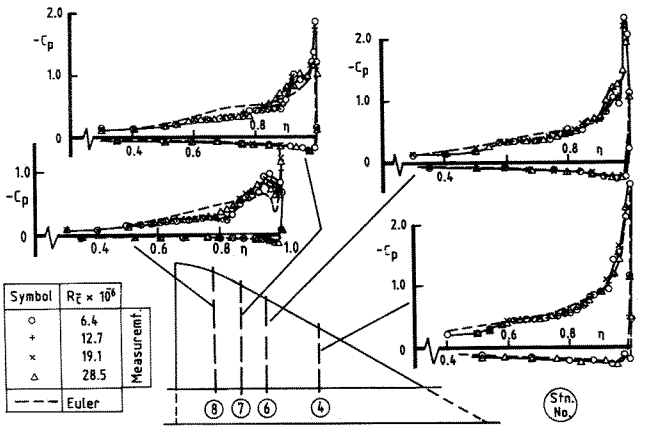

Fig. 10 Effect of Reynolds number on pressure distributions, Wing A, 'leading-edge' trip, $M_\infty = 0.6$, $\alpha = 11.7°$, $C_L = 0.48$.

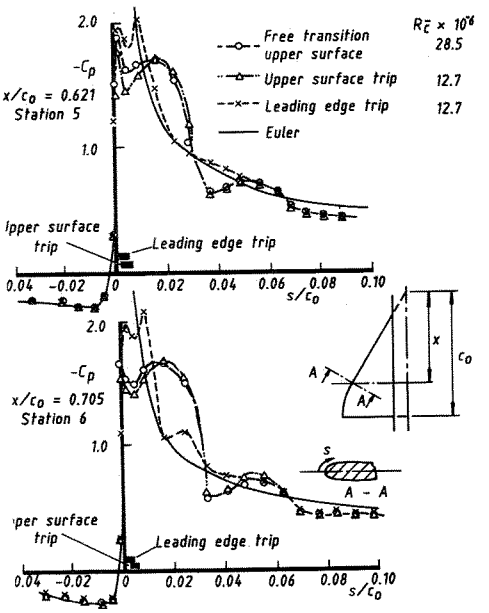

Fig. 11 Comparisons of pressure distributions around leading edge, Wing A, $M_\infty = 0.6$, $\alpha = 11.7°$.

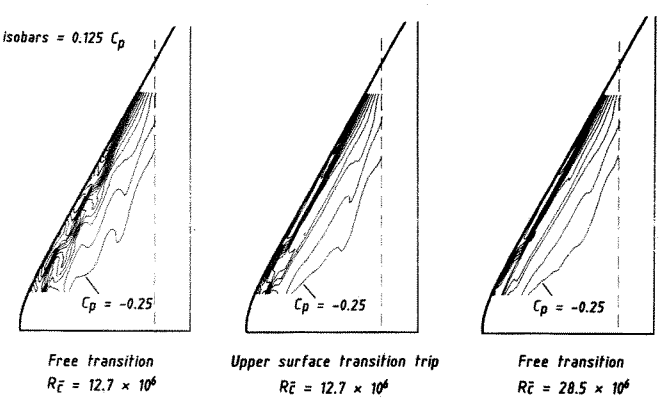

Free transition
$R_{\bar{c}} = 12.7 \times 10^6$

Upper surface transition trip
$R_{\bar{c}} = 12.7 \times 10^6$

Free transition
$R_{\bar{c}} = 28.5 \times 10^6$

Fig. 12 Comparisons of upper-surface isobars, Wing A, $M_\infty = 0.6$, $\alpha = 11.7°$.

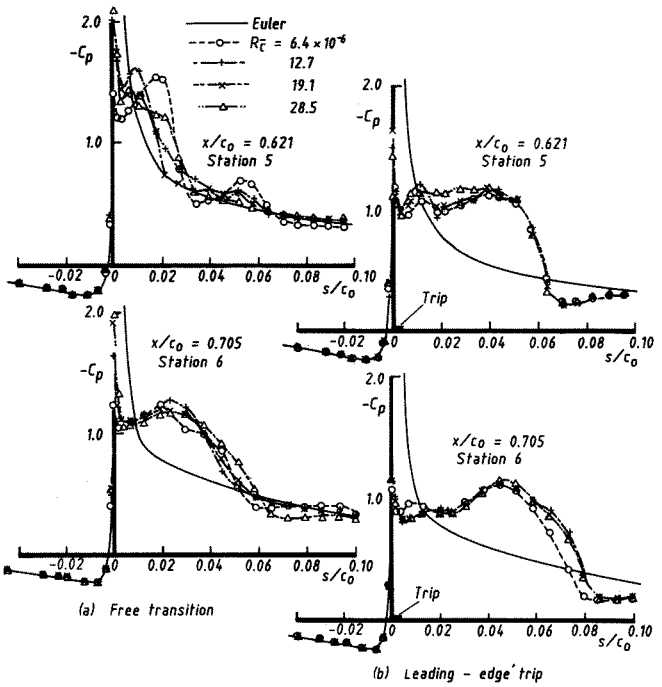

Fig. 13 Pressure distributions around leading edge, Wing C, $M_\infty = 0.6, \alpha = 7^o, C_L = 0.35$.

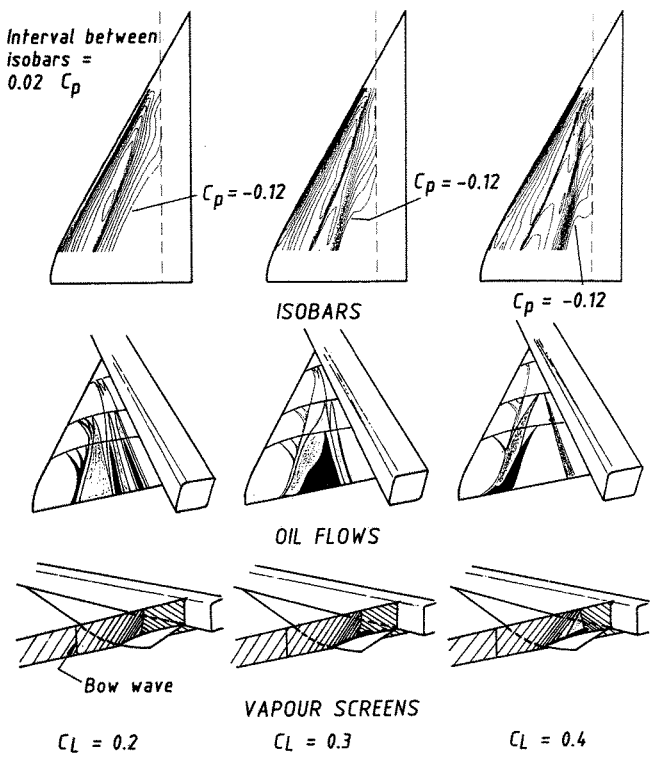

Fig. 14 Data from study of flows over upper surface of Wing A, $M_\infty = 1.61$, $R_{\bar{c}} = 13 \times 10^6$.

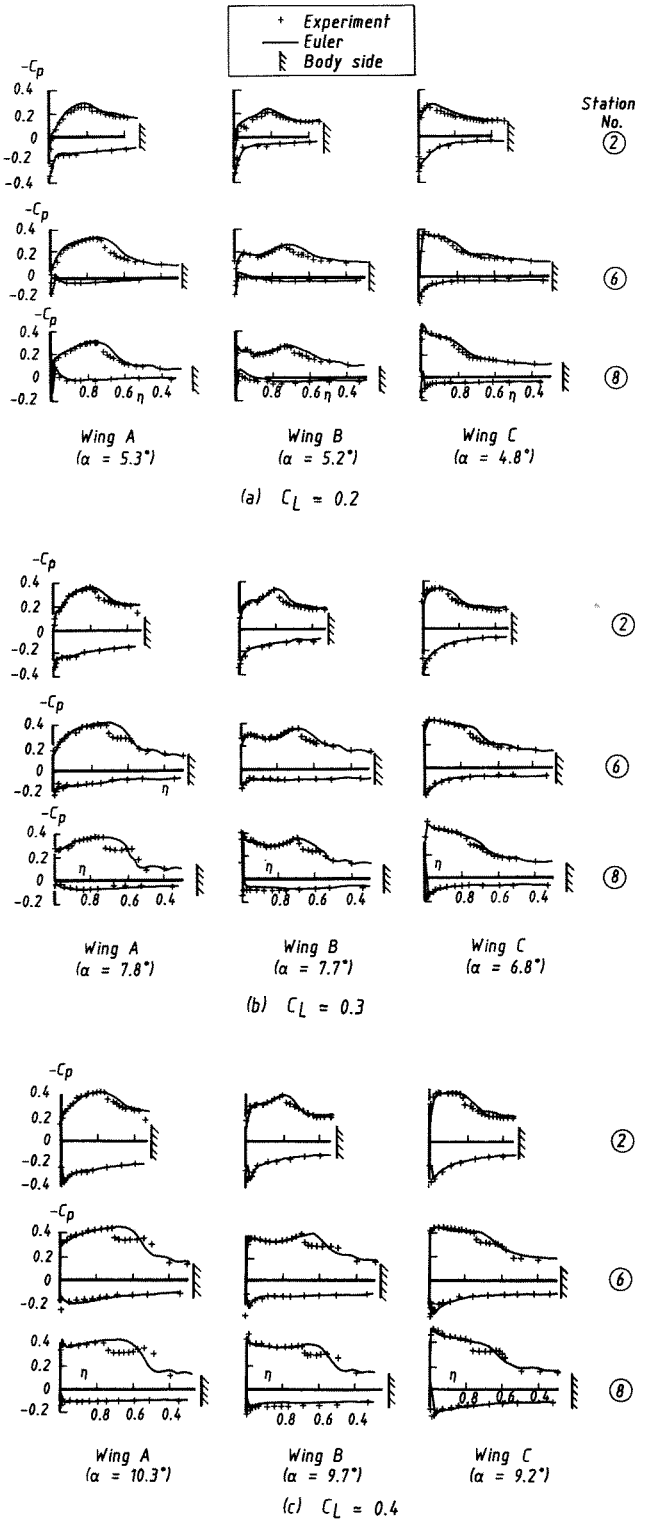

Fig. 15 Pressure distributions, comparison between measurement ($R_{\bar{c}} = 13 \times 10^6$) and prediction, $M_\infty = 1.61$.

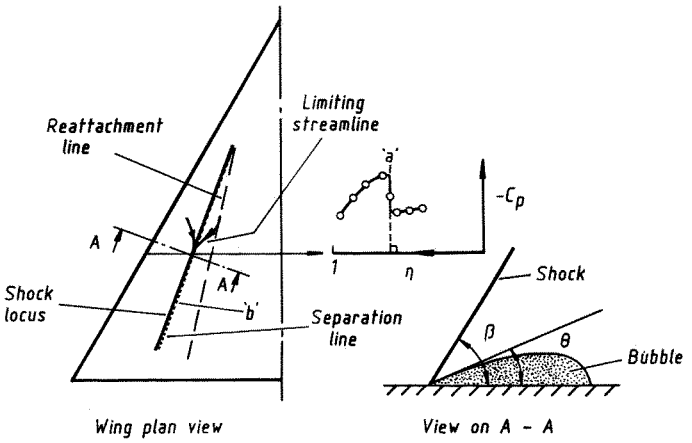

Fig. 16 Definitions for model of shock–induced separation.

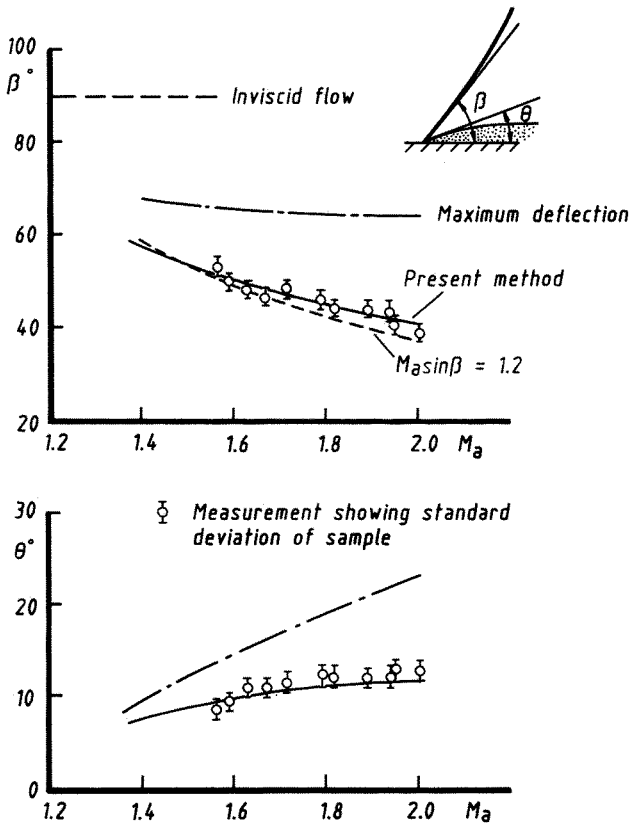

Fig. 17 Comparison between prediction and measurement of shock inclination (β) and flow deflection (θ), Wing A, $M_\infty = 1.61$, $R_c = 13 \times 10^6$.